Structural Transformation of Coassembled Fmoc-Protected Aromatic Amino Acids to Nanoparticles

Tengfei Wang, Cécilia Ménard-Moyon, Alberto Bianco

Structural transformation of co-assembled Fmoc-protected aromatic amino acids to nanoparticles

Tengfei Wang, Cécilia Ménard-Moyon, Alberto Bianco**

CNRS, Immunology, Immunopathology and Therapeutic Chemistry, UPR 3572, University of Strasbourg, ISIS, 67000 Strasbourg, France

Correspondence to: a.bianco@ibmc-cnrs.unistra.fr, c.menard@ibmc-cnrs.unistra.fr

Keywords: nucleation; supramolecular interactions; core-shell structure; hydrophilic-lipophilic balance; crystallization; solvent-switch method; nanofibers

Abstract

Materials made of assembled biomolecules such as amino acids have drawn much attention during the past decades. Nevertheless, research on the relationship between the chemical structure of building block molecules, supramolecular interactions and self-assembled structures is still necessary. Herein, the self-assembly and the co-assembly of fluorenylmethoxycarbonyl (Fmoc)-protected aromatic amino acids (tyrosine, tryptophan and phenylalanine) were studied. The individual self-assembly of Fmoc-Tyr-OH and Fmoc-Phe-OH in water formed nanofibers, while Fmoc-Trp-OH self-assembled into nanoparticles. Moreover, when Fmoc-Tyr-OH or Fmoc-Phe-OH was co-assembled with Fmoc-Trp-OH, the nanofibers were transformed into nanoparticles. UV-Vis, FTIR and fluorescence spectroscopy were used to investigate the supramolecular interactions leading to the self-assembled architectures. π-π Stacking and hydrogen bonding were the main driving forces leading to self-assembly of Fmoc-Tyr-OH and Fmoc-Phe-OH forming nanofibers. Furtherly, a mechanism involving a two-step co-assembly process is proposed based on nucleation and elongation/growth to explain the structure transformation. Fmoc-Trp-OH acted as a fiber inhibitor to alter the molecular interactions in the Fmoc-Tyr-OH or Fmoc-Phe-OH self-assembled structures during the co-assembly process, locking the co-assembly in the nucleation step and preventing the formation of nanofibers. This structure transformation is useful for extending the application of amino acid self- or co-assembled materials to different fields. For example, the amino acids forming nanofibers can be applied for tissue engineering, while they can be exploited as drug nanocarriers when they form nanoparticles.

Introduction

In the context of supramolecular chemistry, the self-assembly of molecules driven by different non-covalent interactions has been deeply exploited during the past decades.[1] Various building blocks, ranging from inorganic and organic molecules to biomacromolecules, can self-assemble. This has impacted many different fields, including biomedicine, materials science, optics, catalysis and energy.[2-4] The functions and features of self-assembled materials depend on each of the individual building block. In addition, the functionalization of these blocks can endow the self-assembled structures with different functionalities. Because of the limitations of artificial/synthetic blocks like low biocompatibility and non-negligible toxicity in applications of self-assembled materials in the biomedical field, more and more focus has been given on biomolecular bricks.[5] Amino acids, fundamental molecules in life, can exhibit the capacity of self-assembly besides their biological functions. Thanks to the advantages of good biocompatibility and easy modification, various nanomaterials formed from the self-assembly of amino acid derivatives have been designed for a wide range of applications, such as drug delivery, 3D cell culture matrix and biosensing.[6-8] The study of the self-assembly process can help to reasonably design amino acid derivatives to regulate the functions and features of the final materials. A typical example is to introduce the Fmoc group into the amino acid structure, which is a common protecting group for amines and widely used in peptide synthesis. By providing additional π-π stacking and hydrophobic interactions, the Fmoc group can improve the self-assembly capacity of amino acids. Indeed, self-assembly studies involving Fmoc-protected amino acids and peptides attracted many attentions in the recent years. For example, Fmoc-protected proline, histidine, alanine and leucine can form nanofibers driven by π-π stacking, hydrogen bonds and hydrophobic interactions, resulting in hydrogels into which silver nanoparticles were synthesized for antibacterial use.[9] In another work, Fmoc-protected cysteine self-assembled into nanoparticles driven by the coordination with Fe^{3+} ions.[10] The nanoparticles exhibited enzyme-like properties when modified by a phthalocyanine-based photosensitizer, and were used for the treatment of hypoxic cancers. Besides, many researches regarding the self-assembly of Fmoc-protected dipeptides were also reported, and their assembly mechanism and potential applications were explored.[11,12] Various dipeptides with Fmoc protection, including Fmoc-diphenylalanine,[13] Fmoc-dialanine,[14] Fmoc-tyrosine-leucine, Fmoc-tyrosine-alanine, Fmoc-tyrosine-serine,[15] can self-assemble into many different structures such as nanoparticles, nanofibers and micelles. Moreover, it is believed that the nature of the peptide side chains can profoundly affect the assembled structures.

Alternative to self-assembly, the co-assembly by two or more components forming one structure has emerged as a robust strategy. Compared with the individual self-assembly, multifunctional materials with enhanced properties can be constructed by introducing building blocks with different functions without additional functionalization. Similarly, the co-assembly of amino acids has also drawn much attention. The co-assembly of amino acid enantiomers, such as $_{L/D}$-phenylalanine and $_{L/D}$-tryptophan, showed enhanced mechanical strength and

different structures, compared to pure enantiomers.[16] Co-assembling drugs or imaging probes with Fmoc-protected amino acids allowed to form materials with a high drug loading efficiency and new properties for diagnosis.[17] All these works emphasize that the powerful co-assembly strategy can have broad application prospects in the biomedical field. Apart from co-assembly, materials assembled by two or more components can also be a result of another aggregation process, which is called self-sorting, depending on the different phase separation modes of the components occurring at the early stage of the assembly process.[18] If each separated phase contains all the components, co-assembly will happen, where the components collectively form one structure, as previously mentioned. In contrast, individual phase separation of each component leads to self-sorting. In this case, each component assembles separately and generates a material with a hybrid structure.[19] Same as the co-assembly, the self-sorting can also regulate the properties of materials, especially hydrogels. For instance, double network hydrogels were formed by self-sorting of photoresponsive peptides and lipids. Due to the self-sorting, the hydrogels could still sustain based on the lipid nanofibers when the peptide nanofibers selectively disassembled under irradiation. Self-sorting helped to generate out-of-equilibrium patterns by reconstruction of disassembled peptide nanofibers in the hydrogels.[20] Self-sorting also enables components to separately *in situ* self-assemble into cells and target different intracellular parts, which is impossible for co-assembly strategies. For instance, by respectively adding targeting moieties of the endoplasmic reticulum and Golgi apparatus to two peptides, the peptide could separately self-assemble *in situ* in the proximity of the two organelles and cause dysfunction.[21] Besides, the interconversion between co-assembly and self-sorting by changing conditions has also been reported. Hydrogels were formed by a non-gelling compound with an alkyl chain of different lengths and a diphenylalanine derivative gelator. The capacity of these two components for self-sorting or co-assembly was dependent on the length of the alkyl chain and the gelation conditions.[18]

Owing to the tunability of non-covalent interactions, the controllable transformation of self-assembled structures shows great potential and advantages.[22] For example, materials formed by the self-assembly of two triblock molecules were found to evolve from micelles to nanofibers upon irradiation at 650 nm. The triblock molecules contained a hydrophobic head (chlorin e6 or bilirubin), a peptide linker and a polyethylene glycol tail.[23] Owing to the presence of chlorin e6, light irradiation led to the generation of reactive oxygen species (ROS), resulting in the degradation of bilirubin and breaking the hydrophobic core of the micelles. Consequently, the material rearranged and formed nanofibers due to the formation of hydrogen bonds between the peptide linkers. Notably, this transformable property gave to the material the capacity to penetrate into solid tumours deeply at the stage of the micellar state, while keeping a long retention time in the tumour due to the transformation into nanofibers after light irradiation, greatly increasing the anticancer effect. Apart from the studies on material properties, studies at the molecular level demonstrated the detailed transforming process of self-assembled structures. Various intermediate structures changing from spherical nanoparticles to nanotubes, then nanofibers and finally solid crystals were observed during the self-assembly process of

Fmoc-3,4-dihydroxyphenylalanine (Fmoc-DOPA). Different supramolecular interactions dominated at these stages and led to the rearrangement of the molecules, such as hydrophobic interactions at the beginning, π-π stacking for the intermediate nanotubes and hydrogen bonds at the crystal stage.[24] Another study detailed the self-assembly process of Fmoc-protected amino acids, and the multiple assembly stages involving the nucleation of nanoparticles and then the elongation into nanofibers.[25] These works described the self-assembly process of single block with spontaneous structure transformation. However, the co-assembly process and the triggered structural transformation involving two Fmoc-protected aromatic amino acids are rarely explored.

π-π Stacking of the aromatic side chains of amino acids can also facilitate the assembly process in addition to interactions with the Fmoc group. For this reason, Fmoc-protected aromatic amino acids, namely Fmoc-Tyr-OH, Fmoc-Trp-OH and Fmoc-Phe-OH, were used as building blocks in this work, aiming to understand both the self- and co-assembly processes.

The molecular assembly was initiated by the solvent-switch method (also called "good-bad solvent"), a general approach for preparing various self-assembled structures.[26] In this strategy, building block molecules are initially dissolved in a "good" solvent as a stock solution, generally at high concentration, in which the blocks are in the free molecular state due to their high solubility in the used solvent. Afterwards, a "bad" solvent is used to dilute the stock solution, and the blocks start to self-assemble because of low solubility. Different "good/bad solvent pairs" can be selected based on the nature of the building blocks. For example, the self-assembly of Fmoc-diphenylalanine could be triggered by dissolving the peptide in 1,1,1,3,3,3-hexafluoro-2-propanol followed by dilution in water, resulting in the formation of hydrogels.[27] Besides, it has been also reported that different Fmoc-protected peptides self-assembled into various structures by dissolving in dimethyl sulfoxide (DMSO) at a high concentration followed by dilution in water.[28] Herein, two different solvent pairs, protic methanol (MeOH)/water and aprotic DMSO/water, were used to study and compare their influence on the assembly process. Firstly, the supramolecular interactions between the Fmoc-protected aromatic amino acids during self-/co-assembly were studied by UV-Vis, attenuated total reflection Fourier transform infrared (ATR-FTIR) and fluorescence spectroscopy, to explore the reasons why these blocks have similar molecular structures, but assembled into different structures. Next, different stages during the assembly were monitored, revealing the different steps of the assembly process and explaining how the structures transformed from nanofibers to nanoparticles after the co-assembly. Finally, based on the obtained results, we propose a possible mechanism about the assembly and structure transformation. This study could help directing molecular design to control the formation of assembled structures and meet various requirements of applications. In addition, the structure transformation capacity of amino acid-based supramolecular materials could greatly extend their properties and broaden their application potentials.[29]

Results and discussion

Self-/co-assembled structures of Fmoc-Tyr-OH, Fmoc-Phe-OH and Fmoc-Trp-OH and structure transformation

The building blocks Fmoc-Tyr-OH, Fmoc-Trp-OH and Fmoc-Phe-OH used in this work contain aromatic side chains (phenol, indole and phenyl, respectively) and the Fmoc group, which greatly enhanced their self-assembly property in water (Figure 1). The self-assembly and co-assembly of these blocks were performed by applying the solvent-switch protocol. For the individual self-assembly of each block, the compound was first dissolved using an organic solvent and then diluted by water. Due to their lower water solubility, the blocks started to assemble. Similarly, the co-assembly was implemented by mixing the stock organic solutions at certain amino acid ratios before dilution in water. Many studies reported that organic solvents of different natures, such as protic or aprotic solvents, could affect the self-assembly behaviour of building blocks by facilitating or inhibiting the formation of non-covalent bonds for instance, generating diverse structures.[30-33] For this reason, two organic solvents, protic MeOH and aprotic DMSO, were individually used to dissolve the amino acid derivatives before water dilution, and the assembled structures generated in these two solvent systems (MeOH/water and DMSO/water) were studied. Transmission electron microscopy (TEM) revealed that in both systems, Fmoc-Tyr-OH and Fmoc-Phe-OH self-assembled into nanofibers with tens of nanometres in width and dozens of micrometres in length, while Fmoc-Trp-OH formed 200-300 nm spherical nanoparticles (Figure 1 and Figure S1a). However, by mixing Fmoc-Trp-OH with Fmoc-Tyr-OH (i.e., binary amino acid nanoparticles, named BAP-Y/W) or Fmoc-Phe-OH (BAP-F/W), the nanofibers transformed into nanoparticles (Figure 1 and Figure S1a). In general, nanofibers can form hydrogels, which can be exploited for tissue engineering, while nanoparticles are widely used as carriers.[34-37] For this reason, this structure transformation gave Fmoc-Tyr-OH and Fmoc-Phe-OH the potential as transporters for drug delivery. Moreover, the same structures generated in the two solvent pairs confirmed that the organic solvents used to dissolve amino acid derivatives had negligible influence on the assembled structures.

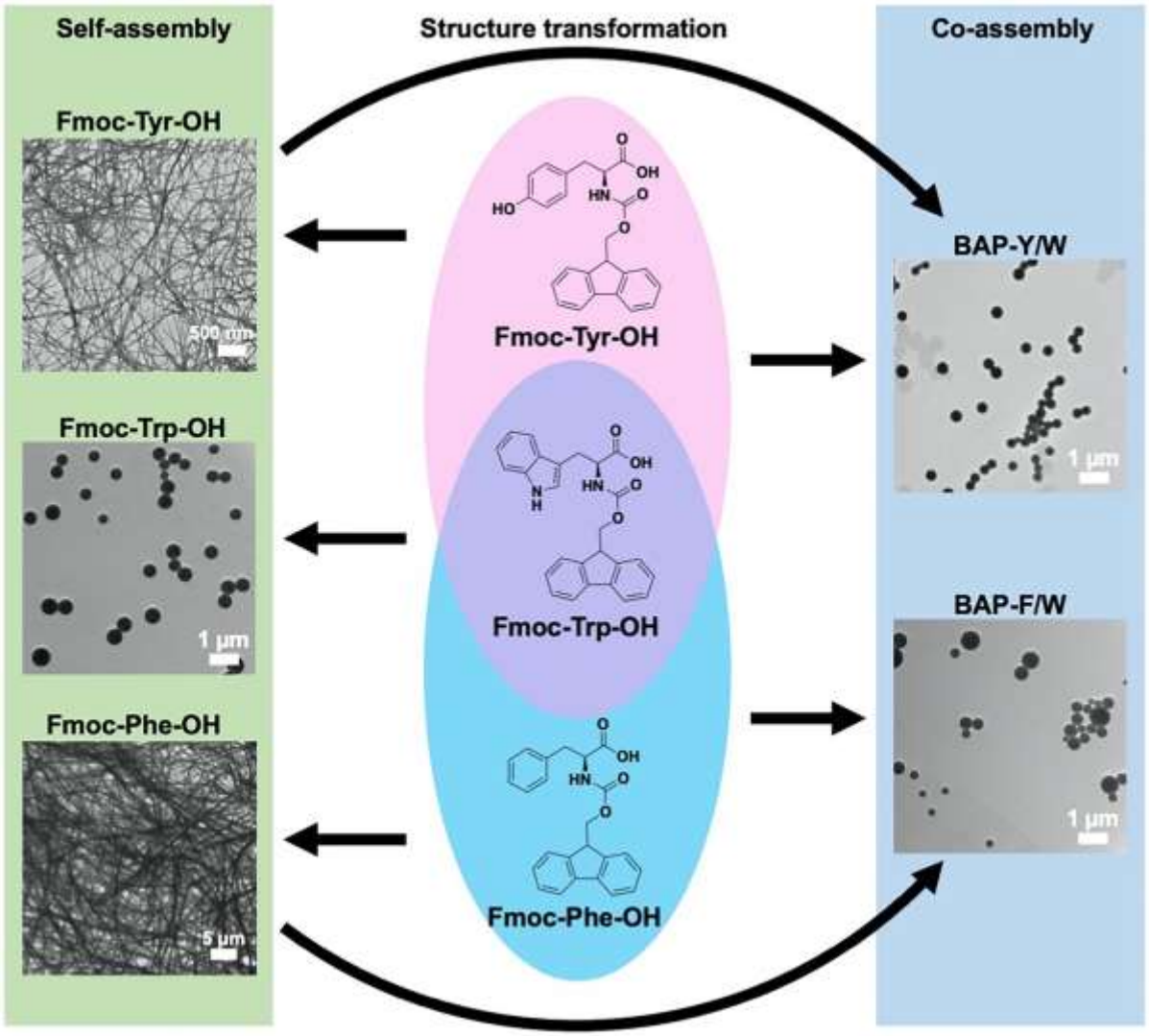

Figure 1. Molecular structures of Fmoc-Tyr-OH, Fmoc-Trp-OH and Fmoc-Phe-OH, and different structures formed from their self-/co-assembly in MeOH/water. Structure transformation of Fmoc-Tyr-OH and Fmoc-Phe-OH after mixing with Fmoc-Trp-OH.

We suggest that Fmoc-Trp-OH drove Fmoc-Tyr-OH and Fmoc-Phe-OH to form the spherical nanoparticles. Interestingly, even a small proportion of Fmoc-Trp-OH in the co-assembly system is able to trigger the structure transformation. The ratios of the amino acid derivatives were changed from 7:3 to 3:7 in BAP-Y/W and BAP-F/W groups, and only nanoparticles were observed (Figure 2a and b). High performance liquid chromatograph (HPLC) was then performed to analyse the composition of BAP-Y/W. The peaks of Fmoc-Tyr-OH and Fmoc-Trp-OH were detected in BAP-Y/W with different block ratios, which confirmed the coexistence of two Fmoc-protected amino acids in the co-assembled structure (Figure S2a). Besides, in order to confirm the generation of nanoparticles was due to the co-assembly rather than self-sorting, a sequential assembly process was performed to intentionally generate self-sorting of the two amino acids and to compare the differences with the co-assembly process.

Fmoc-Tyr-OH was first allowed to self-assemble in water, and then Fmoc-Trp-OH (stock solution in MeOH) was added to this solution for self-assembly. In this case, we observed by TEM that the solution contained both nanofibers and nanoparticles, suggesting the self-sorting of the two amino acids (Figure S2b). Similarly, changing the addition sequence of the two compounds, we still observed the coexistence of both structures (Figure S2c). Hence, no nanofibers were observed in the co-assembly conditions indicating that the two amino acids jointly participated in forming nanoparticles and also confirming that the co-assembly with Fmoc-Trp-OH is critical for the structure transformation of Fmoc-Tyr-OH.

Dynamic light scattering (DLS) analysis was performed to assess the size, polydispersity index (PI) and surface charge of the self-assembled structures. Due to inappropriate mathematical models and correlation function [Supporting Information, Equation (1)], nanofiber-like structures with diverse lengths generally show multiple size populations, and the PI values are usually very high. This is caused by the completely different light scattering pattern of the nanofibers, directly affecting the intensity of the scattered light that is used to calculate the correlation coefficient.[38] The Fmoc-Tyr-OH self-assembled materials showed large values of size and PI (> 0.6) in both MeOH/water and DMSO/water, indicating that the sample was in the form of nanofibers with diverse size populations (Figure 2c and Figure S1b), which was in agreement with TEM. However, BAP-Y/W with different ratios (7:3, 1:1 and 3:7) and the Fmoc-Trp-OH self-assembled group were characterized by 200-300 nm size particles with low PI values (< 0.2), suggesting the formation of homogenous and monodispersed nanoparticles (Figure 2c and Figure S1b). These results were also consistent with the TEM images. Moreover, with the increase of Fmoc-Trp-OH proportion, the size of the nanoparticles slightly increased (Figure 2c). We suppose that this change might result from a lower hydrophilicity of Fmoc-Trp-OH compared to Fmoc-Tyr-OH. Indeed, the indole side chain of Fmoc-Trp-OH is more hydrophobic than the phenol group in Fmoc-Tyr-OH. For this reason, a higher Fmoc-Trp-OH proportion probably led to an enhanced aggregation of the molecules, resulting in larger diameter nanoparticles. We suggest that the hydrophilic-lipophilic balance (HLB) of the building blocks did affect the self-assembly process and the size of the obtained structures. Besides, the surface charge of the self-/co-assembled nanomaterials was also measured (Figure 2d). All materials were characterized by a highly negative surface charge due to the existence of free carboxyl groups. Additionally, the increase of the proportion of Fmoc-Trp-OH led to a more negative surface charge of BAP-Y/W. The DLS analysis was also performed for the assembly of Fmoc-Phe-OH and Fmoc-Trp-OH (Figure 2e and Figure S1b). The Fmoc-Phe-OH self-assembled structures generated in MeOH/water and DMSO/water systems exhibited a big size (~5 μm) with a PI value of 1, corresponding to the maximum PI value, which was indicative of the presence of nanofiber structures. However, the DLS analysis of BAP-F/W with different ratios of Fmoc-Phe-OH and Fmoc-Trp-OH showed 200-300 nm size and very low PI values (< 0.1), confirming the generation of nanoparticles. Contrary to BAP-Y/W, the addition of Fmoc-Trp-OH gradually decreased the size of the nanoparticles (Figure 2e), likely because the indole side chain in Fmoc-Trp-OH was more hydrophilic than the phenyl ring in

Fmoc-Phe-OH. Therefore, higher Fmoc-Phe-OH proportions generated larger nanoparticles. The zeta potential of the self-assembled structures was also highly negative, owing to the presence of the carboxyl groups. Although the surface charge of the Fmoc-Trp-OH nanoparticles was more negative than that of the Fmoc-Phe-OH nanofibers, there were no differences in the zeta potential of the BAP-F/W at different ratios (Figure 2f). The similar hydrodynamic sizes and PI values in MeOH/water and DMSO/water also confirmed that using DMSO instead of MeOH induced no change of the assembled structures.

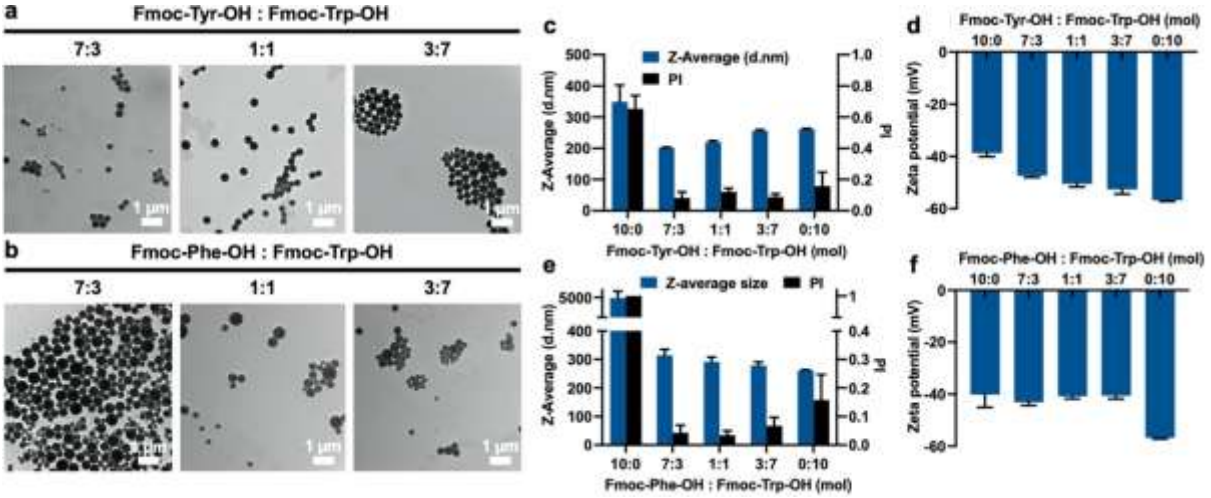

Figure 2. TEM images of the co-assembled structures of (a) BAP-Y/W and (b) BAP-F/W in MeOH/water with different ratios of amino acids. Average size, PI and zeta potential value of (c, d) BAP-Y/W and (e, f) BAP-F/W with different ratios in MeOH/water.

The stability of the assembled structures was subsequently tested in water over 24 h at room temperature (Figure S3a). The solution of self-assembled Fmoc-Tyr-OH formed transparent hydrogels because of the nanofiber structure. However, the individual self-assembled structures of Fmoc-Trp-OH and Fmoc-Phe-OH were unstable in water. A colloidal solution was obtained by Fmoc-Trp-OH self-assembly, but in few hours, aggregation and precipitation occurred. Though hydrogels were obtained during Fmoc-Phe-OH self-assembly, they were stable for only several minutes and then collapsed into a heterogeneous solution. In contrast, BAP-Y/W were more stable than the Fmoc-Trp-OH nanoparticles, demonstrating once again a good colloidal stability for 24 h. This was not the case for the solutions of BAP-F/W, as precipitation was observed. These differences emphasize the significance of HBL for the stability of the assembled structures. Owing to the hydroxyl group in the phenol side chain, Fmoc-Tyr-OH showed a good HLB and a higher hydrophilicity compared to Fmoc-Phe-OH. In the BAP-Y/W nanoparticles, the presence of Fmoc-Tyr-OH could sustain the stability of the nanoparticles in water, which was not the case for Fmoc-Phe-OH in the BAP-F/W nanoparticles. The structures standing for 24 h were also observed by TEM (Figure S3b). Nanofibers were still observed in the Fmoc-Tyr-OH self-assembled hydrogels. The distribution of the fibers after 24 h became more compact and homogeneous, likely due to the stabilization

of the hydrogels over time. Large aggregates with a regular polygon shape was observed in the Fmoc-Trp-OH solution, suggesting crystallization. Besides, after 24-h standing, the nanofibers formed by Fmoc-Phe-OH transformed into wider and straighter nanoribbons with a shorter length, which also indicated crystallization. Indeed, long-time aging of assembled amino acids or peptides water solution is a common approach that is widely used to obtain crystals of these molecules for X-ray studies.[6,39,40] Additionally, a similar phase transition in the self-assembly of Fmoc-pentafluoro-phenylalanine from nanoparticles to gels and then to crystals was also reported.[41] In alignment with the solution photographs, BAP-Y/W still contained nanoparticles after 24-h standing due to their good HLB and water stability, while some crystal-like structures and amorphous aggregates were observed in BAP-F/W group with 24-h standing.

Spectroscopic analysis of the self-/co-assembled structures to understand the supramolecular interactions between blocks

Though the molecular structures of the three Fmoc-protected amino acids are very similar, they self-/co-assembled into different types of structures. In order to explore the assembly mechanism, a spectroscopic analysis was performed to understand the supramolecular interactions between the amino acid building blocks. Firstly, the fluorescence spectra of each self-assembled structure dissolved in MeOH or DMSO at different concentrations were measured (Figure 3 and Figure S4). Similar trends of fluorescence change were shown in both MeOH and DMSO solutions. With the increase of concentration in all the groups, the fluorescence intensity was increased at the beginning, while when the concentration continuously increased, the fluorescence intensity gradually decreased. At the lowest concentrations (0.01-0.1 mg/mL), the molecules most likely freely moved in the solvent and only few supramolecular interactions occurred between the amino acids. Therefore, the fluorescence intensity correlated with the amount of molecules. However, when the concentration increased (0.1-30 mg/mL), the molecules in the solvent became crowded, resulting in supramolecular interactions between the molecules. The negative correlation between the fluorescence intensity and the molecular concentrations resulted from the typical aggregation-caused quenching phenomena, indicating the existence of π-π stacking between the aromatic side chains and Fmoc group.[42] Moreover, a red-shift of the emission peak with increased concentrations was observed in all groups, confirming again the existence of π-π stacking (top inserts in Figure 3 and Figure S4). Indeed, π-π interactions lower the energy level of π electron excited state.[43] Therefore, the emitted fluorescence has less energy and thus presents a red-shift in the emission spectrum. The influence of the solvents on the π-π stacking interactions is little, according to the similar fluorescence changes. The small differences observed between the use of MeOH and DMSO were indicative of a slight solvent effect on the molecular assembly. For example, the maximum fluorescence intensity curves showed that the inflection points of Fmoc-Trp-OH and Fmoc-Phe-OH concentration were 0.1 mg/mL and 1 mg/mL, respectively, when DMSO was used, while they decreased to 0.05 and 0.1 mg/mL, respectively, in MeOH. These results indicated that the minimum critical concentration

required for π-π stacking formation in MeOH was lower than in DMSO (bottom inserts in Figure 3b, c and Figure S4b, c). These results suggest that π-π stacking between Fmoc-amino acids was more favourable in MeOH, although it also occurred in DMSO.

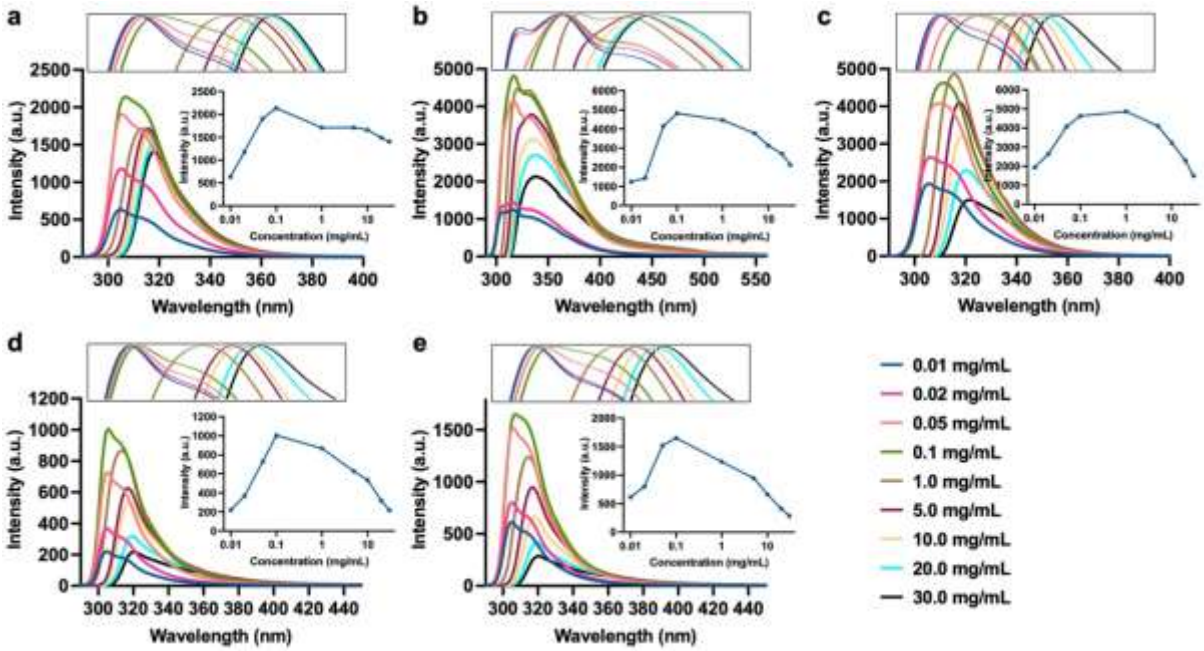

Figure 3. Fluorescence emission spectra of the self-/co-assembled nanostructures dissolved in DMSO at different concentrations. Insets: (top) normalized fluorescence and (bottom) maximum fluorescence intensity for each condition. (a) Fmoc-Tyr-OH, (b) Fmoc-Trp-OH, (c) Fmoc-Phe-OH, (d) BAP-Y/W and (e) BAP-F/W.

In order to obtain the critical self-/co-assembly concentration (CAC) of each building block, a fluorescence probe, 1-anilinonaphthalene-8-sulfonic acid (ANS), which is sensitive to the chemical environment of the binding site, was mixed with the amino acids during the assembly. When the chemical environment of ANS changes from hydrophilic to hydrophobic due to molecular assembly, the fluorescence of ANS sharply rises. Therefore, the building block concentration at the break point of increased ANS fluorescence intensity indicates the CAC.[44,45] In DMSO/water and MeOH/water systems, all the assembly groups showed no change of ANS fluorescence at low amino acid concentrations, whereas the fluorescence intensity was increased sharply as the building block concentration was increased, indicating that the assembly initiated in both solvent systems when the amino acids reached a certain concentration (Figure S5a-e and S6a-e). In DMSO/water system, the CAC of Fmoc-Tyr-OH was 0.2 mg/mL, which was much higher than the other groups (0.04 mg/mL for Fmoc-Trp-OH and BAP-F/W, 0.07 mg/mL for Fmoc-Phe-OH and 0.06 mg/mL for BAP-Y/W) (Figure S5f). Similar CAC values for each group were also obtained in MeOH/water system (0.15 mg/mL for Fmoc-Tyr-OH and ~0.04-0.05 mg/mL for the other groups) (Figure S6f).

Next, UV-Vis absorption spectra of the materials were recorded. Due to the cut-off wavelength of DMSO (265 nm) that overlap with the Fmoc-amino acid absorption peaks, only structures formed from the assembly in MeOH/water were studied. Owing to the existence of the aromatic side chains and the Fmoc group, $\pi \rightarrow \pi^*$ electron transition was observed in the UV region (200-350 nm).[46] The UV-Vis spectra of the Fmoc-protected amino acids and the corresponding amino acids without Fmoc protection in MeOH were obtained to distinguish the absorption peaks in the range of 200-300 nm (Figure S7). The Fmoc group showed the K band at 200-220 nm and the B band at 240-305 nm in all three protected amino acids. The K band is due to the $\pi \rightarrow \pi^*$ transition in the conjugated system, while the B band is characteristic of aromatic moieties and generally appears between 230 and 270 nm.[47] The benzene side chains of H-Phe-OH and Fmoc-Phe-OH showed a low absorbance due to the lack of auxochromic groups and was covered by the absorbance of Fmoc. The K band of the phenol side chains in H-Tyr-OH and Fmoc-Tyr-OH was at ~220 nm, which was partially overlapped with the K band of Fmoc. The K band of the indole side chains in H-Trp-OH and Fmoc-Trp-OH was also located at ~220 nm, with a higher intensity than that of the phenol group. Next, in order to study the interactions between the different building blocks, the absorption peaks of each group in MeOH (no assembly) and MeOH/water (assembly) were compared. In Fmoc-Tyr-OH and Fmoc-Phe-OH groups, the K band of the Fmoc group showed blue shift (~5 nm) when self-assembly occurred in MeOH/water (Figure S8a, c and g). This likely indicated that the Fmoc group in these two molecules underwent *H*-aggregation during the self-assembly process, indicating an ordered face-to-face stacking (Figure S8f).[48,49] *H*- and *J*-aggregation are two types of molecular π-π stacking patterns. *H*-aggregates correspond to face-to-face arrangements, accompanied by a blue shift of the absorption spectra. In the case of *J*-aggregation, molecules stack in a head-to-tail manner and the absorption spectra show a red shift.[50,51] However, in the Fmoc-Trp-OH and the two BAP groups, the K band of Fmoc showed no shift in MeOH/water (Figure S8b, d, e and g). Considering the nanofibers formed by Fmoc-Tyr-OH and Fmoc-Phe-OH, we can speculate that the *H*-aggregation of the Fmoc group played a significant role in forming the nanofibers. Because of a relatively higher free energy, *H*-aggregation is not the most favourable type of stacking.[52] Therefore, *H*-aggregation might require the combined action from other interactions, such as hydrogen bonding, to make the whole system in an energy favourable arrangement. We suggest that when Fmoc-Trp-OH is mixed with Fmoc-Tyr-OH or Fmoc-Phe-OH and co-assembled in water, the *H*-aggregation of the Fmoc group in Fmoc-Tyr-OH or Fmoc-Phe-OH is altered and the assembled structures change.

Additionally, ATR-FTIR spectroscopy was also used to study the assembly mechanism. After forming aggregates in deuterated water, a shift of the peak at 1600-1800 cm^{-1}, corresponding to the stretching vibration of the carbonyl groups, was observed for all groups when compared with deuterated DMSO (DMSO-d_6) or deuterated MeOD (MeOD-d_4) conditions, in which the Fmoc-amino acid derivatives were soluble (Figure 4a-e and Figure S9).[53] The shift of this peak in water suggested the formation of hydrogen bonds between the O atom of the carbonyl group and the –OH group of the carboxylic acid or the phenol of tyrosine, or the –NH group in the

urethane of the Fmoc or the indole of tryptophan during the assembly process in water.[54,55] Indeed, a shift of FTIR peaks to lower wavenumbers is generally indicative of increased intermolecular forces.[56] The larger shift was observed for Fmoc-Tyr-OH and Fmoc-Phe-OH compared to Fmoc-Trp-OH, BAP-Y/W and BAP-F/W (Figure 4f and Figure S9). The small or large shifts indicated the variety of hydrogen bonds leading to the formation of different self-assembled materials, nanofibers for Fmoc-Tyr-OH and Fmoc-Phe-OH, and nanoparticles for Fmoc-Trp-OH and the BAP composed of Fmoc-Trp-OH and Fmoc-Tyr-OH or Fmoc-Phe-OH. Besides, the similar case, in which the shift in the nanofiber groups was larger than that of the nanoparticle groups, was also obtained in MeOD-d_4/D_2O, but the shift space in this condition was smaller than that in DMSO/D_2O (e.g., ~12 cm^{-1} in MeOD-d_4/D_2O vs. ~50 cm^{-1} in DMSO/D_2O for Fmoc-Tyr-OH), indicating that the solvents may have some effects on hydrogen bonds, probably attributed to the hydrogen bond breaker nature of DMSO.[57,58] Moreover, the existence of a hydrogen bond network can also explain the much higher CACs of Fmoc-Tyr-OH than that of other groups (Figure S5f and S6f). DMSO or MeOH could competitively form hydrogen bonds with blocks, which impacted the generation of intermolecular hydrogen bonds between Fmoc-Tyr-OH, hindering their self-assembly. In general, we suggest that the hydrogen bonds play an important role in the formation of the Fmoc-Tyr-OH and Fmoc-Phe-OH nanofibers, probably participating to the *H*-aggregation of the Fmoc groups. We hypothesize that the addition of Fmoc-Trp-OH induces a structure transformation by altering the hydrogen bond network in the self-assembly of Fmoc-Tyr-OH or Fmoc-Phe-OH alone.

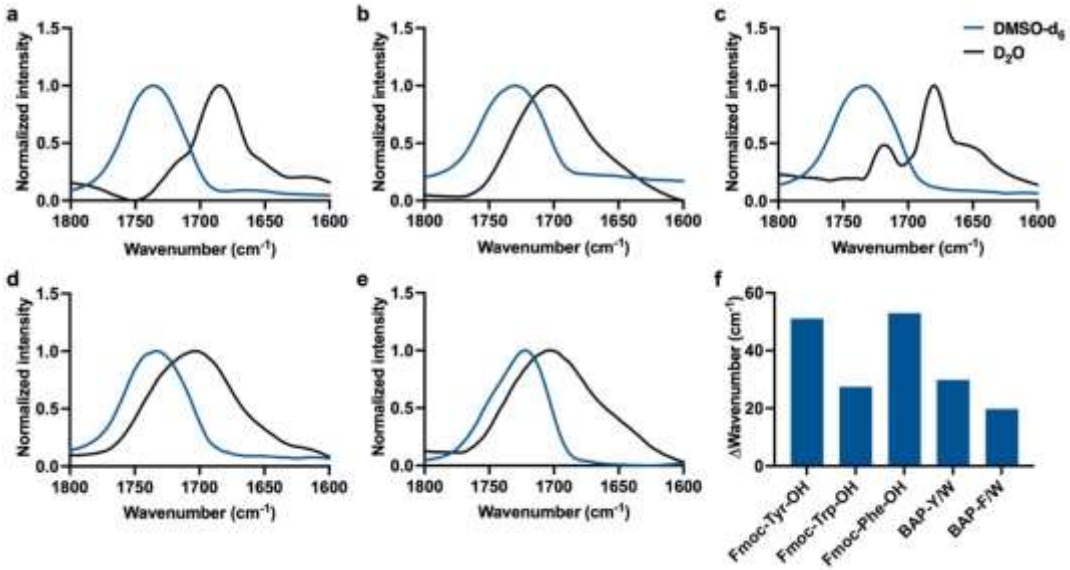

Figure 4. ATR-FTIR spectra of the amino acid derivatives solubilized in DMSO-d_6 and aggregated in DMSO-d_6/D_2O. (a) Fmoc-Tyr-OH, (b) Fmoc-Trp-OH, (c) Fmoc-Phe-OH, (d) BAP-Y/W and (e) BAP-F/W. (f) Shift of the wavenumber of the carbonyl stretching vibration peak in the different groups.

Overall, from the structural studies and spectroscopic analyses, we can suggest that the assembly of the amino acid derivatives was driven by combined supramolecular interactions, including π-π stacking, hydrogen bonds and hydrophobic interactions. The different hydrogen bond arrangements and the type of aromatic group in the lateral chain of the amino acids had a crucial influence on the formation of nanofibers or nanoparticles, while MeOH or DMSO only showed limited effect on the molecular interactions and no change on the final structures.

Monitoring of the self-/co-assembly process over time

We furtherly monitored the carbonyl peak shift of the Fmoc-amino acids and binary mixtures in solution by ATR-FTIR spectroscopy over a period of time. The amino acid derivatives were dissolved in DMSO-d_6 or MeOD-d_4 (molecular state) and aggregated in D_2O (supramolecular state). Firstly, in DMSO-d_6/D_2O system, FTIR spectrum of Fmoc-Tyr-OH showed the peak of the carbonyl group shifted from 1736 cm^{-1} in DMSO-d_6 to 1696 cm^{-1} after the addition of D_2O (at 0 min), indicating the initiation of the self-assembly (Figure 5a). The peak gradually shifted after 2 min to a lower wavelength (1684 cm^{-1}) after 4 min. Similarly, the peak of the carbonyl group also shifted from 1730 to 1704 cm^{-1} upon addition of D_2O in the deuterated DMSO solution of Fmoc-Trp-OH, but no further shift was observed over time (Figure 5b). The carbonyl peak of Fmoc-Phe-OH showed a behaviour similar to Fmoc-Tyr-OH (Figure 5c). In contrast, the peak shifts in both BAP groups were similar to that observed for Fmoc-Trp-OH (Figure 5d and e). Note that the peak shift at the first 2 min in the two nanofiber groups (Fmoc-Tyr-OH and Fmoc-Phe-OH) showed a similar position as the peak shift in the nanoparticle groups, suggesting the generation of intermediate nanoparticle (INP) structures at the early stage of the nanofiber formation. After 2 min, the peaks in the nanofiber groups continued moving to large shifts, while the small shift stopped in the nanoparticle groups. The progressive peak shift in the nanofiber formation indicated that the formation process contained more than one stage: the INPs formed at the initial stage and then transformed into nanofibers. However, only the nanoparticle stage existed in the Fmoc-Trp-OH and co-assembled groups. Moreover, in the co-assembly groups, same peak shifts as Fmoc-Trp-OH were observed, suggesting that the presence of Fmoc-Trp-OH locked the second peak shift process (originally exist in self-assembly of Fmoc-Tyr-OH and Fmoc-Phe-OH) in the binary systems, indicating that the transformation from INPs to nanofibers was hampered, finally generating the structure transformation to nanoparticles. Next, the same time-dependent shift of the carbonyl peaks was also observed in MeOD-d_4/D_2O system, including INP formation and nanofiber transformation in Fmoc-Tyr-OH and Fmoc-Phe-OH groups (Figure S10). This confirmed that the change of the organic solvent had no impact on the assembly process. However, the peak shift in MeOD-d_4/D_2O only lasted 120 sec, which was faster than the self-assembly in DMSO-d_6/D_2O. This could be due to more interference of DMSO than MeOH on the hydrogen bond formation, which slowed down the assembly process. For this reason, we decided to monitor the self-assembly process in the rest of the study in DMSO/water system, which could give us enough time to characterize each stage.

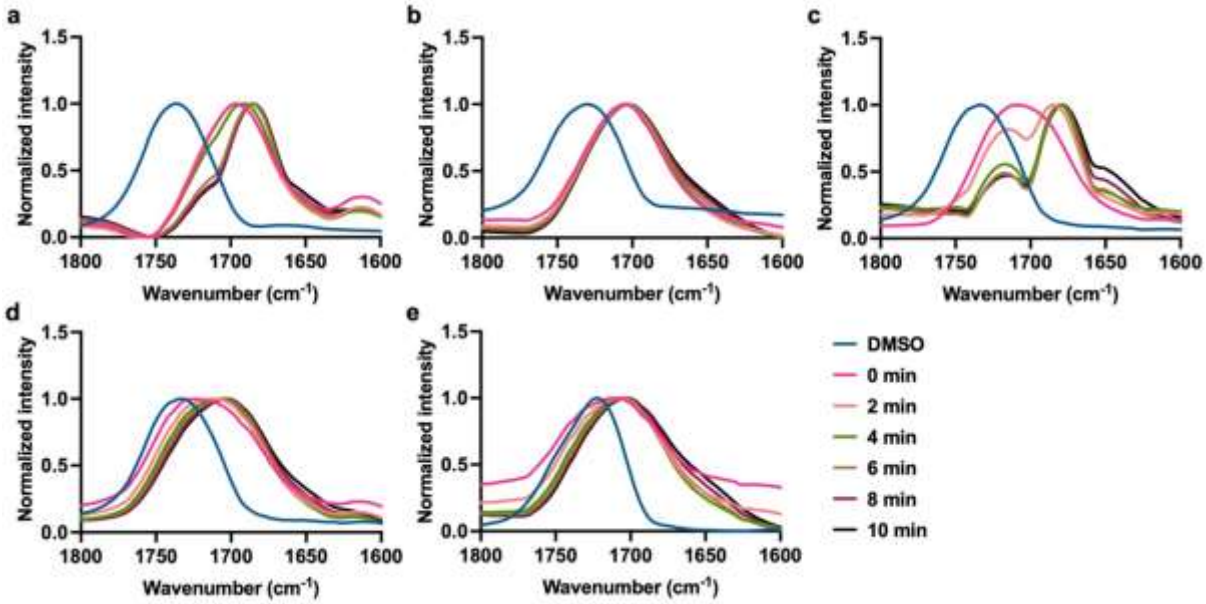

Figure 5. FTIR spectra with different time points of a DMSO-d_6 solution of (a) Fmoc-Tyr-OH, (b) Fmoc-Trp-OH, (c) Fmoc-Phe-OH, (d) BAP-Y/W and (e) BAP-F/W upon addition of D_2O (0 min) and evolution of the spectra over a period of 10 min.

The assembly process was monitored at different times, and different states were observed (Figure S11). At the beginning of the Fmoc-Tyr-OH self-assembly, a white colloidal solution was observed (Figure S11a, 0 min), which turned gradually into a transparent solution, suggesting the formation of INPs at the beginning of self-assembly. Notably, after 2 min, some white materials were still observed, but at a lower concentration than that at 0 min, suggesting the formed INPs (see below) were unstable and transformed rapidly into nanofibers. When this solution was kept overnight, a transparent hydrogel was formed (Figure S3). To form a hydrogel, the length and density of the nanofibers have to achieve a certain level. Therefore, we can conclude that the growth of the nanofibers arising from the self-assembly of Fmoc-Tyr-OH was slow, contrarily to Fmoc-Phe-OH forming a gel after 6 min (Figure S11b). The different behaviours of Fmoc-Tyr-OH and Fmoc-Phe-OH highlight the crucial role of the phenolic hydroxyl group, which increased the HLB and provided a denser hydrogen bond network in the Fmoc-Tyr-OH assembled structures. In contrast, in the case of Fmoc-Phe-OH, the hydrophobic interactions and π-π stacking dominated the self-assembly process, as also supported by the lower CAC of Fmoc-Phe-OH in comparison to Fmoc-Tyr-OH (Figure S5f and Figure S6f). Though the INP transformation to nanofibers was still observed, the faster aggregation process of Fmoc-Phe-OH disfavoured the formation of an ordered hydrogel, which finally collapsed. In the case of Fmoc-Trp-OH and the two BAP groups, a colloidal solution was observed without any visual change over time from 0 to 22 min, suggesting the formation of stable nanoparticles (Figure S11c-e). The addition of Fmoc-Trp-OH to Fmoc-Tyr-OH and Fmoc-Phe-OH allowed preventing the formation of nanofibers leading to the formation of hydrogels. This conclusion was supported by DLS analysis. Over the period of 22 min, the size

of the Fmoc-Tyr-OH self-assembled structures showed little changes, while the PI values sharply increased after 2 min (Figure S12). At 0 and 2 min, the size was ~200 nm and the PI was below 0.3. This indicated the formation of INPs at this early stage. However, the PI dramatically increased to ~1 at 4 min, time at which the solution became transparent, indicating the transformation of the INPs into nanofibers. In the case of Fmoc-Phe-OH, though the size and PI of the self-assembled structures increased gradually over time, no drastic increase in PI and size was observed until 10 min. At 0-4 min, time period at which a colloidal solution was observed (Figure S11b), the size was ~250 nm and the PI ~0.1, indicating the presence of INPs. After 10 min, when the hydrogel became transparent (Figure S11b), the size sharply increased to several micrometers, and the PI increased to ~1, indicating the transformation from INPs to nanofibers (Figure S12). For the Fmoc-Trp-OH and two BAP groups, the size of the nanoparticles increased slightly from ~200 to ~300 nm for Fmoc-Trp-OH and BAP-Y/W and to ~400 nm for BAP-F/W, while the PI value was less than 0.3 (Figure S12). No sharp increase in size and PI was measured meaning that the systems maintained the structure of nanoparticles. These results are in alignment with the FTIR results (Figure 5), confirming the existence of INPs that can transform into nanofibers in Fmoc-Tyr-OH and Fmoc-Phe-OH groups.

Structural analyses by high-resolution transmission electron microscopy coupled to energy dispersive X-ray spectroscopy

A more detailed structural information was provided by high-resolution transmission electron microscopy (HRTEM). The nanoparticle groups, including Fmoc-Trp-OH, BAP-Y/W and BAP-F/W, were observed (Figure S13). The nanoparticles obtained from the self-assembly of single Fmoc-Trp-OH showed solid and homogeneous spherical structures, while two parts with a different contrast were observed in the binary nanoparticles. BAP-Y/W demonstrated a core-shell structure with a higher contrast core and lower contrast shell, while patches with a lower contrast were distributed unevenly on the BAP-F/W surface. These results indicated that the distribution of the two components in these binary nanoparticles might be heterogeneous. To understand their distribution, the locations of Fmoc-Tyr-OH and Fmoc-Trp-OH in BAP-Y/W was subsequently studied by energy dispersive X-ray (EDX) spectroscopy mapping. For this purpose, Fmoc-3,5-diiodo-Tyr-OH and Fmoc-5-fluoro-Trp-OH (Figure S14) were used instead of Fmoc-Tyr-OH and Fmoc-Trp-OH, respectively, to allow distinct mapping of both amino acids by EDX owing to the fluorine and iodine atoms. The same core-shell nanoparticle structures were also observed in Fmoc-3,5-diiodo-Tyr-OH/Fmoc-5-fluoro-Trp-OH co-assembled groups and by using only one type of halogenated Fmoc-protected amino acid (Fmoc-3,5-diiodo-Tyr-OH/Fmoc-Trp-OH and Fmoc-Tyr-OH/Fmoc-5-fluoro-Trp-OH co-assembled groups) (Figure 6a). Therefore, there was no structural change induced by the use of halogen-labelled Fmoc-amino acids, confirming that the presence of the fluorine and iodine atoms in the amino acid side chains had no influence on the co-assembly process. Then, the amount of fluorine and iodine in the HRTEM images was assessed by EDX. The F/I atom ratio was ~1:2, which was consistent with the 1:1 ratio of the two building blocks, indicating that

the core-shell nanoparticles were constituted of the two amino acids (Figure 6b). Next, the distribution of the two molecules was determined by EDX mapping. We could observe that the distribution of Fmoc-5-fluoro-Trp-OH was homogeneous in the whole nanoparticles, while the Fmoc-3,5-diiodo-Tyr-OH was more localized in the core (Figure 6c). The relative amount of the two amino acids was detected along the white line in Figure 6c, showing that the amount of Fmoc-3,5-diiodo-Tyr-OH sharply increased in the core of the nanoparticles (Figure 6d). We hypothesize that the higher localization of Fmoc-Tyr-OH in the core and the presence of Fmoc-Trp-OH in the shell certainly prevent Fmoc-Tyr-OH from interacting with other Fmoc-Tyr-OH molecules, thus hampering the formation of nanofibers.

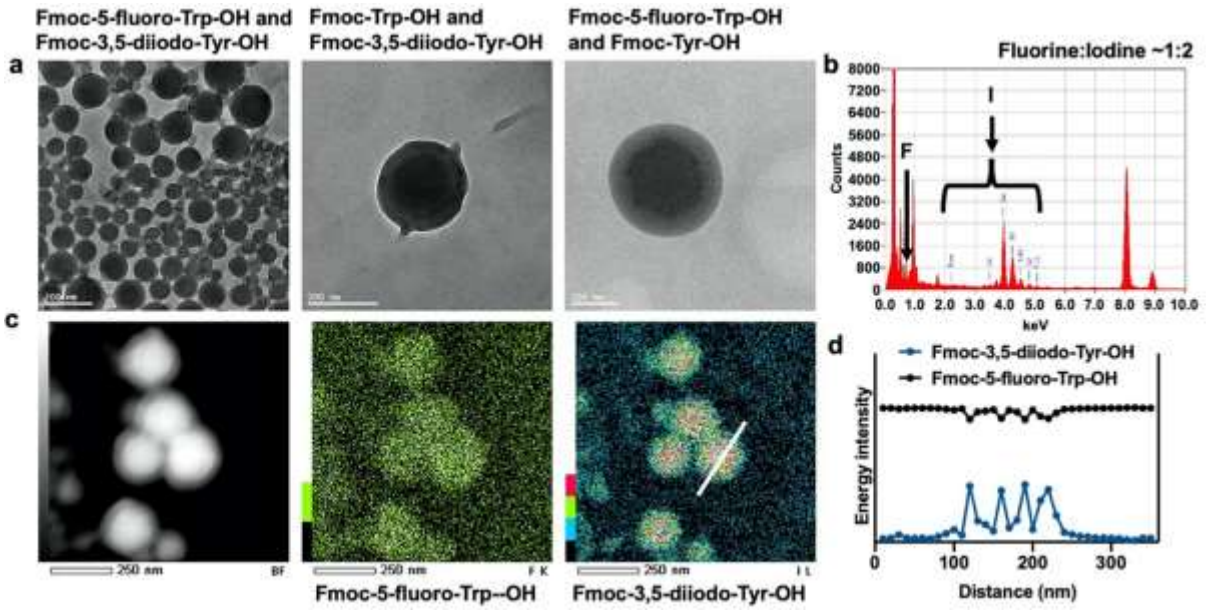

Figure 6. (a) HRTEM images of the co-assembled nanoparticles made of (left) Fmoc-3,5-diiodo-Tyr-OH and Fmoc-5-fluoro-Trp-OH, (middle) Fmoc-3,5-diiodo-Tyr-OH and Fmoc-Trp-OH, and (right) Fmoc-Tyr-OH and Fmoc-5-fluoro-Trp-OH, respectively. (b) EDX showing the amount of fluorine and iodine. (c) Dark field image and EDX mapping of the co-assembled nanoparticles made of Fmoc-3,5-diiodo-Tyr-OH and Fmoc-5-fluoro-Trp-OH. (d) Distribution of Fmoc-3,5-diiodo-Tyr-OH and Fmoc-5-fluoro-Trp-OH in the nanoparticles assessed by EDX mapping along the white line.

Proposed self-assembly and co-assembly mechanisms

Based on the possible supramolecular interactions between the selected Fmoc-protected amino acids, we propose that the self-assembly of Fmoc-Tyr-OH, Fmoc-Trp-OH and Fmoc-Phe-OH firstly underwent a fast nucleation process mainly driven by π-π stacking and hydrophobic interactions, generating INPs at the beginning of the self-assembly, followed by a transformation into nanofibers for Fmoc-Tyr-OH and Fmoc-Phe-OH (Figure 7a). The structural transformation was monitored using DLS and FTIR spectroscopy, indicating that the formation of nanofibers resulted from the elongation of INPs morphologies. The blue shift of the absorbance peaks in the UV-Vis spectra of nanofiber groups suggested a *H*-aggregation of the Fmoc group, while hydrogen bonding was confirmed by FTIR spectroscopy. These

interactions specifically detected in Fmoc-Tyr-OH and Fmoc-Phe-OH led to the transformation of the INPs and nanofiber generation. It has been previously reported that multiple intermediate structures were successively generated and transformed along with changing the domination of supramolecular interactions (e.g., hydrophobic interactions, aromatic stacking and hydrogen bonds) during the assembly process of Fmoc-DOPA.[24] Moreover, a similar mechanism was also proposed by Yan *et al.*, in which the Fmoc-protected histidine, Fmoc-protected alanine or carboxybenzyl-protected diphenylalanine dipeptide self-assembled into nanofibers following a similar two-step process.[25] In contrast, in the case of Fmoc-Trp-OH, the different supramolecular interactions triggered only the nucleation step of the molecule and did not evolve to well-ordered molecular arrangements, thus leading to the formation of nanoparticles.

In the co-assembly systems, the presence of Fmoc-Trp-OH altered the self-assembly of Fmoc-Tyr-OH and Fmoc-Phe-OH. The peak shift, suggesting the transformation of the INPs into nanofibers, observed in the FTIR spectra during the co-assembly process stopped, thus locking the system at the INPs stage (Figure 7b). The EDX mapping demonstrated the homogenous distribution of Fmoc-Trp-OH in the whole structure, while Fmoc-Tyr-OH was mainly located in the core, probably indicating that the addition of Fmoc-Trp-OH stabilized the intermediate nanoparticles by enveloping Fmoc-Tyr-OH and prevented from interacting with other Fmoc-Tyr-OH molecules. Meanwhile, the hydrogen bond network or *H*-aggregation were not detected in these groups, suggesting that the interaction of Fmoc-Trp-OH with Fmoc-Tyr-OH limited these supramolecular interactions. The lack of these essential interactions also caused the assembly process to remain at the intermediate spherical nanoparticle stage. Indeed, some recent studies revealed that the tryptophan residue could act as a fiber-structure inhibitor, converting many fiber-like structures into nanoparticles when the tryptophan residue was introduced into the peptide sequences.[59-62] For example, it was reported that a special motif called tryptophan zipper generated by cross-standing pairing of indole rings played an important role in retarding nanofiber formation, leading to the formation of nanoparticles.[59] These studies support why we hypothesize that the INP stage was locked by Fmoc-Trp-OH in our binary assembly system.

The nucleation and growth process of our building blocks could be explained by different theories.[63] The self-assembly of Fmoc-Trp-OH leading to the formation of nanoparticles probably follows the LaMer mechanism, proposing that the nucleation and growth process can be divided into three stages: 1) a sharp increase of the building block concentration in solution; 2) a burst-nucleation of the building blocks to an infinite rate and a significant decrease of the free building blocks in solution; and 3) a growth of the nanoparticles by the building block diffusion.[64] Indeed, the number of the building blocks in water increased rapidly by adding the Fmoc-Trp-OH stock solution. Then, the hydrophobic interactions, due to the high hydrophobicity of Fmoc-Trp-OH, and the π-π stacking triggered a fast aggregation of the amino acids, ensuring the burst-nucleation. This process was confirmed by the appearance of the Fmoc-Trp-OH solution at 0 min as a white colloidal solution and by DLS at 0 min (Figure S11c

and Figure S12a). In the third stage of the growth, because of the decreased concentration of free Fmoc-Trp-OH in solution and an inefficient diffusion, the growth was slowed down. The DLS analysis showed that the size of the Fmoc-Trp-OH nanoparticles increased slowly over time (Figure S12a). In contrast, we suggest that the nanofibers (Fmoc-Tyr-OH or Fmoc-Phe-OH) were formed by the Ostwald ripening, a process in which small particles are redissolved to form larger structures.[65] The photographs of the Fmoc-Tyr-OH and Fmoc-Phe-OH solutions at the beginning of the process showed the formation of white colloidal solutions that disappeared over time (Figure S11a and b), probably due to redissolution. Moreover, the INP size was larger than the diameter of the nanofibers according to TEM images and DLS at 0 min (Figure 1, Figure S1a and Figure S12a), which could be an indication of the elongation stage of the nanofibers based on the dissolution of the INPs and rearrangement of the blocks. For the co-assembly process with structure transformation, the locking of the INP stage could result in the aggregation of Fmoc-Trp-OH and Fmoc-Tyr-OH (or Fmoc-Phe-OH) before INP dissolution, thus preventing the INPs from redissolution, stopping the following Ostwald ripening and eventually leading to the LaMer mechanism. A similar slow size growth of BAP-Y/W and BAP-F/W shown by DLS supported the assembly process switched to the LaMer mechanism (Figure S12a).

Additionally, due to the high hydrophobicity of the amino acids, which leads to an imbalance of hydrophilicity and lipophilicity, the assembled nanostructures showed a low water stability and underwent different fates after standing in water for 24 h (Figure S3 and 7c). The BAP-Y/W nanoparticles were more stable in water compared to the BAP-F/W nanoparticles, because the presence of Fmoc-Tyr-OH improved the HLB of the binary system, emphasizing the importance of the balance between hydrophilicity and lipophilicity in providing a good water stability.

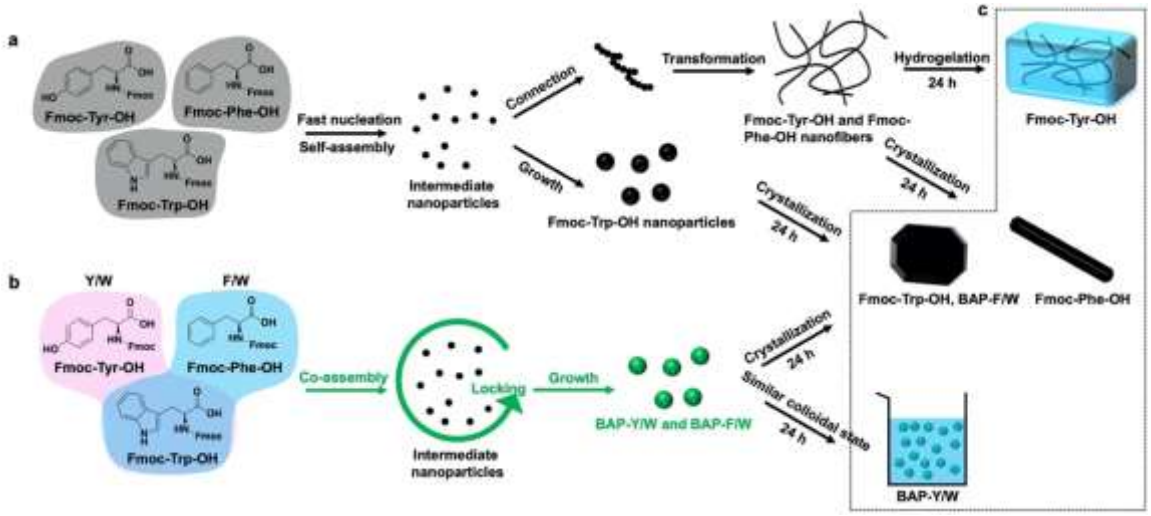

Figure 7. Possible mechanism of (a) the self-assembly process and (b) the rapid structure transformation in the co-assembly systems. (c) Fate of the nanostructures after 24-h standing in ambient conditions.

Conclusions

This study as evidenced that, while Fmoc-Tyr-OH and Fmoc-Phe-OH self-assemble into nanofibers, nanoparticles can be generated by the co-assembly with Fmoc-Trp-OH. This structure transformation indicated that Fmoc-Trp-OH can modulate the self-assembly of Fmoc-protected amino acids. Different supramolecular interactions, including π-π stacking, hydrophobic interactions and hydrogen bonding, collectively participated in the assembly process to different extents. The stacking of the Fmoc group and a dense network of hydrogen bonds were specifically detected in the self-assembly of Fmoc-Tyr-OH and Fmoc-Phe-OH into nanofibers. A 'two-step' process based on the nucleation of intermediate nanoparticles and their elongation/growth is proposed. The co-assembly with Fmoc-Trp-OH locks the nucleation stage of Fmoc-Tyr-OH and Fmoc-Phe-OH, localizing the molecules in the core and stopping the elongation into nanofibers. Our study provides an understanding of the relationship between the structural properties and supramolecular interactions of amino acid building blocks, allowing to control self-assembly. The capacity of structure transformation of the assembled amino acids offers opportunities for various applications, in particular in nanomedicine. We are currently exploiting BAP-Y/W as drug carriers in cancer therapy. Multifunctional nanoparticles can be designed through the loading of different drugs and surface modification for combined anticancer therapy to efficiently eliminate tumours.

Experimental Section

Materials: Fmoc-Tyr-OH was purchased from Bachem Holding AG, Fmoc-Trp-OH and Fmoc-Phe-OH from Sigma-Aldrich, and Fmoc-5-fluoro-Trp-OH and Fmoc-3,5-diiodo-Tyr-OH were purchased from Iris Biotech GmbH. 1-anilinonaphthalene-8-sulfonic acid (ANS) was purchased from Fisher Scientific. Methanol (MeOH), dimethyl sulfoxide (DMSO) and acetonitrile were purchased from VWR international. D_2O, MeOD-d_4 and DMSO-d_6 were purchased from Eurisotop. The water used in this work was Milli-Q® water.

Preparation of self-/co-assembled nanostructures by a solvent-switch method: The amino acids were dissolved in MeOH or DMSO at 25 mg/mL concentration (stock solution), which was diluted 100 times by adding 1 mL of water to initiate self-assembly after homogeneous mixing. For the co-assembly, mixed stock solutions were prepared first (25 mg/mL in MeOH or DMSO) and the co-assembly was performed by diluting the mixed stock solution 100 times in water with homogeneous mixing. Except where otherwise stated, BAP-Y/W and BAP-F/W mentioned in this work are co-assembled at 1:1 ratio.

Characterization of self-/co-assembled nanostructures: The co-assembled nanomaterials were dissolved in MeOH for analysis by high performance liquid chromatograph (HPLC) (e2695 Alliance, Waters Corporation, 220 nm detector, Nucleosil 100-5 Waters C18 reverse-

phase HPLC column). The column was used with a 1.2 mL/min flow rate of a gradient from 0 to 100% of B (A = H_2O/0.1% trifluoroacetic acid (TFA); B = CH_3CN/0.08% TFA) for 20 min. Transmission electron microscopy (TEM) (H-7500, Hitachi) with an accelerating voltage of 75 kV and AMT Hamamatsu digital camera (Hamamatsu Photonics, Hamamatsu City) was used to observe the nanostructures. The sample solutions were dropped on a copper grid (Formvar film 300 Mesh, Cu from Electron Microscopy Sciences) and dried under ambient environment. High resolution TEM (HRTEM) (2100F, JEOL) under 200 kV coupled to energy dispersive X-ray (EDX) spectroscopy of voltage was used to observe the detailed structure of the nanoparticles. Fmoc-3,5-diiodo-Tyr-OH and Fmoc-5-fluoro-Trp-OH were used to replace Fmoc-Tyr-OH and Fmoc-Trp-OH. The fluorine and iodine act as the label to determine the distribution of Fmoc-Tyr-OH and Fmoc-Trp-OH under EDX mapping. The size, polydispersity index (PI) and surface charge of the materials were assessed by dynamic light scattering (DLS) (Zetasizer Lab, Malvern Panalytical). The correlation function used by DLS measurement is equation (1):

$$G_k(\tau_k) = \sum_{i=0} I(t_i)\, I(t_i + \tau_k) \quad (1)$$

Where G is the correlation coefficient; τ is the delay time; t is the time and I is the intensity of scattering light.

CAC measurement of the self-/co-assembled nanostructure: ANS powder was dissolved in block stock solutions (in MeOH or DMSO) at concentration of 4mM, and the solution was diluted by water to initiate the assembly of blocks according to the previously mentioned solvent-switch method. By controlling the concentration of block in stock solution, samples with different final concentrations of block were prepared and the final concentration of ANS in samples remained at 40 μM. After 10 min incubation, the fluorescence of samples was detected using fluorescence spectroscopy (FP-8300, JASCO) with the excitation wavelength at 360 nm.

Spectroscopic analysis of the self-/co-assembled nanostructures: For the analysis by UV-Vis spectroscopy (Cary 5000, Agilent Technologies), the amino acid solutions at 0.1 mg/mL final concentration were prepared in pure MeOH, and the assembled groups with the same concentration were prepared by solvent-switch method. The absorbance between 200-350 nm was measured. For the fluorescence spectroscopy, the amino acids were dissolved in 1 mL of DMSO or MeOH at the concentrations of 0.01, 0.02, 0.05, 0.1, 1, 5, 10, 20 and 30 mg/mL and excited at 265 nm. For the ATR-FTIR spectroscopy (Nicolet™ 6700, Thermo Scientific, equipped with a diamond ATR polarization accessory), the amino acids were dissolved in DMSO-d_6 or MeOD-d_4 followed by the addition of D_2O (organic solvent/D_2O: 1/9, v/v) to prepare the self-/co-assembled structures. The signal from 525 to 4000 cm^{-1} was recorded.

Supporting Information

TEM images and PI of self-/co-assembled structures, HPLC chromatograms and TEM images of self-sorting structures, photographs of self-/co-assembled nanomaterial solutions and their TEM images, fluorescence emission spectra of Fmoc-amino acids, fluorescence intensity of ANS mixed with Fmoc-amino acids, UV-Vis absorption spectra of amino acids, ATR-FTIR spectra of Fmoc-amino acids, size and PI of the different self-/co-assembled structures, HRTEM images of the nanoparticles.

Acknowledgements

This work was supported by the Centre National de la Recherche Scientifique (CNRS), by the Agence Nationale de la Recherche (ANR) through the LabEx project Chemistry of Complex Systems (ANR-10-LABX-0026_CSC) and by Jean-Marie Lehn Foundation. The authors wish to thank Cathy Royer from the "Plateforme Imagerie In Vitro de l'ITI Neurostra" CNRS UAR 3156, University of Strasbourg (Strasbourg, France) for TEM analysis, Dr. Dris Ihiawakrim from the Transmission Electron Microscopy Platform at the IPCMS (Strasbourg, France) for the HRTEM analyses and Yilin He for her help with ATR-FTIR spectroscopy. T. Wang is indebted to the Chinese Scholarship Council for supporting his PhD internship.

Conflict of interest

The authors declare no conflict of interest.

References

[1] Zhang, S.-G. Fabrication of Novel Biomaterials through Molecular Self-Assembly, *Nat. Biotechnol.* 2003, **21**, 1171-1178.

[2] Gao, J.; Zhan, J.; Yang, Z.-M. Enzyme-Instructed Self-Assembly (EISA) and Hydrogelation of Peptides, *Adv. Mater.* 2020, **32**, 1805798.

[3] Galeotti, F.; Pisco, M.; Cusano, A. Self-Assembly on Optical Fibers: A Powerful Nanofabrication Tool for Next Generation "Lab-on-Fiber" Optrodes, *Nanoscale* 2018, **10**, 22673-2270.

[4] Li, C.; Li, Q.; Kaneti, Y. V.; Hou, D.; Yamauchi, Y.; Mai, Y.-Y. Self-Assembly of Block Copolymers towards Mesoporous Materials for Energy Storage and Conversion Systems, *Chem. Soc. Rev.* 2020, **49**, 4681-4736.

[5] Wang, L.; Gong, C.-C.; Yuan, X.-Z.; Wei, G. Controlling the Self-Assembly of Biomolecules into Functional Nanomaterials through Internal Interactions and External Stimulations: A Review, *Nanomaterials* 2019, **9**, 285.

[6] Xing, P.-Y.; Phua, S. Z. F.; Wei, X.; Zhao, Y.-L. Programmable Multicomponent Self-Assembly Based on Aromatic Amino Acids, *Adv. Mater.* 2018, **30**, 1805175.

[7] Mandal, D.; Mandal, S. K.; Ghosh, M.; Das, P. K. Phenylboronic Acid Appended Pyrene-Based Low-Molecular-Weight Injectable Hydrogel: Glucose-Stimulated Insulin Release, *Chem. Eur. J.* 2015, **21**, 12042-12052.

[8] Wang, T.-F.; Ménard-Moyon, C.; Bianco, A. Self-Assembly of Amphiphilic Amino Acid Derivatives for Biomedical Applications, *Chem. Soc. Rev.* 2022, **51**, 3535-3560.

[9] Song, J.-W.; Yuan, C.-Q.; Jiao, T.-F.; Xing, R.-R.; Yang, M.-Y.; Adams, D. J.; Yan, X.-H. Multifunctional Antimicrobial Biometallohydrogels Based on Amino Acid Coordinated Self-Assembly, *Small* 2020, **16**, 1907309.

[10] Li, Y.-X.; Sun, P.; Zhao, L.-Y.; Yan, X.-H.; Dennis, K. P. N.; Lo, P.-C. Ferric Ion Driven Assembly of Catalase-like Supramolecular Photosensitizing Nanozymes for Combating Hypoxic Tumors, *Angew. Chem.* 2020, **132**, 23428-23438.

[11] Tao, K.; Levin, A.; Adler-Abramovich, L.; Gazit, E. Fmoc-Modified Amino Acids and Short Peptides: Simple Bio-Inspired Building Blocks for the Fabrication of Functional Materials, *Chem. Soc. Rev.* 2016, **45**, 3935-3953.

[12] Li, L.-C.; Xie, L.; Zheng, R.-L.; Sun, R.-Q. Self-Assembly Dipeptide Hydrogel: The Structures and Properties, *Front. Chem.* 2021, **9**, 739791.

[13] Sadownik, J. W.; Leckie, J.; Ulijn, R. V. Micelle to Fibre Biocatalytic Supramolecular Transformation of an Aromatic Peptide Amphiphile, *Chem. Commun.* 2011, **47**, 728-730.

[14] Mu, X.-J.; Eckes, K. M.; Nguyen, M. M.; Suggs, L. J.; Ren, P.-Y. Experimental and Computational Studies Reveal an Alternative Supramolecular Structure for Fmoc-Dipeptide Self-Assembly, *Biomacromolecules* 2012, **13**, 3562-3571.

[15] Bai, S.; Pappas, C.; Debnath, S.; Frederix, P. W. J. M.; Leckie, J.; Fleming, S.; Ulijn, R. V. Stable Emulsions Formed by Self-Assembly of Interfacial Networks of Dipeptide Derivatives, *ACS Nano* 2014, **8**, 7005-7013.

[16] Bera, S.; Xue, B.; Rehak, P.; Jacoby, G.; Ji, W.; Shimon, L. J. W.; Beck, R.; Král, P.; Cao, Y.; Gazit, E. Self-Assembly of Aromatic Amino Acid Enantiomers into Supramolecular Materials of High Rigidity, *ACS Nano* 2020, **14**, 1694-1706.

[17] Zhang, H.; Liu, K.; Li, S.-K.; Xin, X.; Yuan, S.-L.; Ma, G.-H.; Yan, X.-H. Self-Assembled Minimalist Multifunctional Theranostic Nanoplatform for Magnetic Resonance Imaging-Guided Tumor Photodynamic Therapy, *ACS Nano* 2018, **12**, 8266-8276.

[18] Panja, S.; Dietrich, B.; Smith, A. J.; Seddon, A.; Adams, D. J. Controlling Self-Sorting versus Co-assembly in Supramolecular Gels, *ChemSystemsChem* 2022, **4**, e202200008.

[19] Safont-Sempere, M. M.; Fernández, G.; Würthner, F. Self-Sorting Phenomena in Complex Supramolecular Systems, *Chem. Rev.* 2011, **111**, 5784-5814.
[20] Nakamura, K.; Tanaka, W.; Sada, K.; Kubota, R.; Aoyama, T.; Urayama, K.; Hamachi, I. Phototriggered Spatially Controlled Out-of-Equilibrium Patterns of Peptide Nanofibers in a Self-Sorting Double Network Hydrogel, *J. Am. Chem. Soc.* 2021, **143**, 19532-19541.
[21] Liu, X.; Li, M.-M.; Liu, J.-Z.; Song, Y.-Q.; Hu, B.-B.; Wu, C.-X.; Liu, A.-A.; Zhou, H.; Long, J.-F.; Shi, L.-Q.; Yu, Z.-L. In Situ Self-Sorting Peptide Assemblies in Living Cells for Simultaneous Organelle Targeting, *J. Am. Chem. Soc.* 2022, **144**, 9312-9323.
[22] Long, Y.-Y.; Song, H.-M.; He, B.; Lai, Y.-S.; Liu, R.; Long, C.-Y.; Gu, Z.-W. Supramolecular Self-assembly of Monoend-Functionalized Methoxy Poly(ethylene glycol) and α-Cyclodextrin : From Micelles to Hydrogl, *J. Biomater. Appl.* 2012, **27**, 333-344.
[23] Liu, R.; Yu, M.-N.; Yang, X.-T.; Umeshappa, C. S.; Hu, C.; Yu, W.-Q.; Qin, L.; Huang, Y.; Gao, H.-L. Linear Chimeric Triblock Molecules Self-Assembled Micelles with Controllably Transformable Property to Enhance Tumor Retention for Chemo-Photodynamic Therapy of Breast Cancer, *Adv. Funct. Mater.* 2019, **29**, 1808462.
[24] Fichman, G.; Guterman, T.; Damron, J.; Adler-Abramovich, L.; Schmidt, J.; Kesselman, E.; Shimon, L. J. W.; Ramamoorthy, A.; Talmon, Y.; Gazit, E. Spontaneous Structural Transition and Crystal Formation in Minimal Supramolecular Polymer Model, *Sci. Adv.* 2016, **2**, e1500827.
[25] Yuan, C.-Q.; Levin, A.; Chen, W.; Xing, R.-R.; Zou, Q.-L.; Herling, T. W.; Challa, P. K.; Knowles, T. P. J.; Yan, X.-H. Nucleation and Growth of Amino Acid and Peptide Supramolecular Polymers through Liquid-Liquid Phase Separation, *Angew. Chem. Int. Ed.* 2019, **58**, 18116-18123.
[26] Dognini, P.; Coxon, C. R.; Alves, W. A.; Giuntini, F. Peptide-Tetrapyrrole Supramolecular Self-Assemblies: State of the Art, *Molecules* 2021, **26**, 693.
[27] Mahler, A.; Reches, M.; Rechter, M.; Cohen, S.; Gazit, E. Rigid, Self-Assembled Hydrogel Composed of a Modified Aromatic Dipeptide, *Adv. Mater.* 2006, **18**, 1365-1370.
[28] Orbach, R.; Adler-Abramovich, L.; Zigerson, S.; Mironi-Harpaz, I.; Seliktar, D.; Gazit, E. Self-Assembled Fmoc-Peptides as a Platform for the Formation of Nanostructures and Hydrogels, *Biomacromolecules* 2009, **10**, 2646-2651.
[29] Zhang, W.-B.; Gao, C.-Y. Morphology Transformation of Self-Assembled Organic Nanomaterials in Aqueous Solution Induced by Stimuli-Triggered Chemical Structure Changes, *J. Mater. Chem. A* 2017, **5**, 16059-16104.
[30] Janni, D. S.; Reddy, U. C.; Saroj, S.; Muraleedharan, K. M. A Modular Approach towards Drug Delivery Vehicles Using Oxanorbornane-Based Non-Ionic Amphiphiles, *J. Mater. Chem. B* 2016, **4**, 8025-8032.
[31] Korevaar, P. A.; Schaefer, C.; Greef, T. F. A.; Meijer, E. W. Controlling Chemical Self-Assembly by Solvent-Dependent Dynamics, *J. Am. Chem. Soc.* 2012, **134**, 13482-13491.
[32] Wang, J.; Liu, K.; Yan, L.-Y.; Wang, A.-H.; Bai, S.; Yan, X.-H. Trace Solvent as a Predominant Factor to Tune Dipeptide Self-Assembly, *ACS Nano* 2016, **10**, 2138-2143.
[33] Chen, K.-Y.; Jiao, T.-F.; Li, J.-K.; Han, D.-X.; Wang, R.; Tian, G.-J.; Peng, Q.-M. Chiral Nanostructured Composite Films via Solvent-Tuned Self-Assembly and Their Enantioselective Performances, *Langmuir* 2019, **35**, 3337-3345.
[34] Mitchell, M. J.; Billingsley, M. M.; Haley, R. M.; Wechsler, M. E.; Peppas, N. A.; Langer, R. Engineering Precision Nanoparticles for Drug Delivery, *Nat. Rev. Drug Discov.* 2021, **20**, 101-124.
[35] Soppimath, K. S.; Aminabhavi, T. M.; Kulkarni, A. R.; Rudzinski, W. E. Biodegradable Polymeric Nanoparticles as Drug Delivery Devices, *J. Control. Release* 2001, **70**, 1-20.
[36] Lee, K. Y.; Mooney, D. J. Hydrogels for Tissue Engineering, *Chem. Rev.* 2001, **101**, 1869-1880.

[37] Khademhosseini, A.; Langer, R. Microengineered Hydrogels for Tissue Engineering, *Biomaterials* 2007, **28**, 5087-5092.
[38] Kätzel, U.; Vorbau, M.; Stintz, M.; Gottschalk-Gaudig, T.; Barthel, H. Dynamic Light Scattering for the Characterization of Polydisperse Fractal Systems: II. Relation between Structure and DLS Results, *Part. Part. Syst. Charact.* 2008, **25**, 19-30.
[39] Xue, S.-X.; Zhang, N.; Hu, X.-L.; Zeng, Y.-F.; Zhang, J.-B.; Xing, P.-Y.; Zhao, Y.-L. Self-Assembly Evolution of N-Terminal Aromatic Amino Acids with Transient Supramolecular Chirality, *J. Phys. Chem. Lett.* 2020, **11**, 1490-1496.
[40] Xing, P.-Y.; Chen, H.-Z.; Xiang, H.-J.; Zhao, Y.-L. Selective Coassembly of Aromatic Amino Acids to Fabricate Hydrogels with Light Irradiation-Induced Emission for Fluorescent Imprint, *Adv. Mater.* 2018, **30**, 1705633.
[41] Cohen-Gerassi, D.; Arnon, Z. A.; Guterman, T.; Levin, A.; Ghosh, M.; Aviv, M.; Levy, D.; Knowles, T. P. J.; Shacham-Diamand, Y.; Adler-Abramovich, L. Phase Transition and Crystallization Kinetics of a Supramolecular System in a Microfluidic Platform, *Chem. Mater.* 2020, **32**, 8342-8349.
[42] Zong, L.-Y.; Xie, Y.-J.; Wang, C.; Li, J.-R.; Li, Q.-Q.; Li, Z. From ACQ to AIE: The Suppression of the Strong π-π Interaction of Naphthalene Diimide Derivatives through the Adjustment of Their Flexible Chains, *Chem.Commun.* 2016, **52**, 11496-11499.
[43] Yang, L.; Wang, X.-J.; Zhang, G.-Z.; Chen, X.-F.; Zhang, G.-Q.; Jiang, J. Aggregation-Induced Intersystem Crossing: A Novel Strategy for Efficient Molecular Phosphorescence, *Nanoscale* 2016, **8**, 17422-17426.
[44] Diaferia, C.; Roviello, V.; Morelli, G.; Accardo, A. Self-Assembly of PEGylated Diphenylalanines into Photoluminescent Fibrillary Aggregates, *ChemPhysChem* 2019, **20**, 2774-2782.
[45] Ashwanikumar, N.; Plaut, J. S.; Mostofian, B.; Patel, S.; Kwak, P.; Sun, C.; McPhail, K.; Zuckerman, D. M.; Esener, S. C.; Sahay, G. Supramolecular Self-Assembly of Nanodrill-Like Structures for Intracellular Delivery, *J. Control. Release* 2018, **282**, 7689.
[46] Shi, W.-L.; Guo, F.; Li, M.-Y.; Shi, Y.; Tang, Y.-B. N-Doped Carbon Dots/CdS Hybrid Photocatalyst That Responds to Visible/Near-Infrared Light Irradiation for Enhanced Photocatalytic Hydrogen Production, *Sep. Purif. Technol.* 2019, **212**, 142-149.
[47] Yadav, L. D. S. Ultraviolet (UV) and Visible Spectroscopy. In: Organic Spectroscopy, Springer, Dordrecht 2005, 7-51.
[48] Zhai, D.-T.; Xu, W.; Zhang, L.-Y.; Chang, Y.-T. The Role of "Disaggregation" in Optical Probe Development, *Chem. Soc. Rev.* 2014, **43**, 2402-2411.
[49] Yan, Z.-Q.; Xu, H.-Y.; Guang, S.-Y.; Zhao, X.; Fan, W.-L.; Li, X.-Y. A Convenient Organic-Inorganic Hybrid Approach Toward Highly Stable Squaraine Dyes with Reduced H-Aggregation, *Adv. Funct. Mater.* 2012, **22**, 345-352.
[50] Deng, Y.-H.; Yuan, W.; Jia, Z.; Liu, G. H- and J-Aggregation of Fluorene-Based Chromophores, *J. Phys. Chem. B* 2014, **118**, 14536-14545.
[51] Más-Montoya, M.; Janssen, R. A. J. The Effect of H- and J-Aggregation on the Photophysical and Photovoltaic Properties of Small Thiophene-Pyridine-DPP Molecules for Bulk-Heterojunction Solar Cells, *Adv. Funct. Mater.* 2017, **27**, 1605779.
[52] Qi, J.-P.; Hu, X.-W.; Dong, X.-C.; Lu, Y.; Lu, H.-P.; Zhao, W.-L.; Wu, W. Towards More Accurate Bioimaging of Drug Nanocarriers: Turning Aggregation-Caused Quenching into a Useful Tool, *Adv. Drug Deliv. Rev.* 2019, **143**, 206-225.
[53] Edington, S. C.; Flanagan, J. C.; Baiz, C. R. An Empirical IR Frequency Map for Ester C=O Stretching Vibration, *J. Phys. Chem. A* 2016, **120**, 3888-3896.
[54] Nugrahani, I.; Utami, D.; Permana, B.; Ibrahim, S. Development of the NSAID-L-Proline Amino Acid Zwitterionic Cocrystals, *J. Appl. Pharm. Sci.* 2018, **8**, 057-063.

[55] Löbmann, K.; Laitinen, R.; Strachan, C.; Rades, T.; Grohganz, H. Amino Acids as Co-Amorphous Stabilizers for Poorly Water-Soluble Drugs - Part 2: Molecular Interactions, *Eur. J. Pharm. Biopharm.* 2013, **85**, 882-888.
[56] Yang, Z.-H.; Yin, T.-H.; Zhang, F.-F.; Wu, W.; Lin, M.-Q.; Dong, Z.-X.; Zhang, J. Investigation on Dispersion Properties of CO_2 and Ester Solvent Mixtures Using in Situ FTIR Spectroscopy, *RSC Adv.* 2020, **10**, 18192-18199.
[57] Bao, Y.; Huang, X.-B.; Xu, J.; Cui, S.-X. Effect of Intramolecular Hydrogen Bonds on the Single-Chain Elasticity of Poly(vinyl alcohol): Evidencing the Synergistic Enhancement Effect at the Single-Molecule Level, *Macromolecules* 2021, **54**, 7314-7320.
[58] Qian, L.; Guo, X.; Zhang, K.; Yu, M. Effects of Hydrogen Bonds on the Single-Chain Mechanics of Chitin, *Phys. Chem. Chem. Phys.* 2022, **24**, 24535-24541.
[59] Dolai, G.; Shill, S.; Roy, S.; Mandal, B. Atomic Insight on Inhibition of Fibrillization of Dipeptides by Replacement of Phenylalanine with Tryptophan, *Langmuir* 2023, **39**, 9367-9383.
[60] Viswanathan, G.-K.; Paul, A.; Gazit, E.; Segal, D. Naphthoquinone Tryptophan Hybrids: A Promising Small Molecule Scaffold for Mitigating Aggregation of Amyloidogenic Proteins and Peptides, *Front. Cell Dev. Biol.* 2019, **7**, 242.
[61] Paul, A.; Frenkel-Pinter, M.; Alvarez, D. E.; Milordini, G.; Gazit, E.; Zacco, E.; Segal, D. Tryptophan-Galactosylamine Conjugates Inhibit and Disaggregate Amyloid Fibrils of Aβ42 and hIAPP Peptides while Reducing Their Toxicity, *Commun. Biol.* 2020, **3**, 484.
[62] Paul, A.; Li, W.-H.; Viswanathan, G. K.; Arad, E.; Mohapatra, S.; Li, G.; Jelinek, R.; Gazit, E.; Li, Y.-M.; Segal, D. Tryptophan-Glucosamine Conjugates Modulate Tau-Derived PHF6 Aggregation at Low Concentrations, *Chem. Commun.* 2019, **55**, 14621-14624.
[63] Thanh, N. T. K.; Maclean, N.; Mahiddine, S. Mechanisms of Nucleation and Growth of Nanoparticles in Solution, *Chem. Rev.* 2014, **114**, 7610-7630.
[64] LaMer, V. K.; Dinegar, R. H. Theory, Production and Mechanism of Formation of Monodispersed Hydrosols, *J. Am. Chem. Soc.* 1950, **72**, 4847-4854.
[65] Ostwald, W. On the Assumed Isomerism of Red and Yellow Mercury Oxide and the Surface-Tension of Solid Bodies, *Z. Phys. Chem.* 1900, **34**, 495-503.